ACS Catalysis

RESEARCH ARTICLE

pubs.acs.org/acscatalysis

Improving the Carbon Resistance of Ni-Based Steam Reforming Catalyst by Alloying with Rh: A Computational Study Coupled with Reforming Experiments and EXAFS Characterization

Jiahua Guo,[†,‡] Chao Xie,[†,§] Kyungtae Lee,[∥] Neng Guo,[⊥] Jeffrey T. Miller,[⊥] Michael J. Janik,[*,∥] and Chunshan Song[*,†,‡,∥]

[†]Clean Fuels and Catalysis Program, EMS Energy Institute, 209 Academic Projects Building, The Pennsylvania State University, University Park, Pennsylvania 16802, United States

[‡]Department of Energy & Mineral Engineering, [§]Department of Materials Science and Engineering, and [∥]Department of Chemical Engineering, The Pennsylvania State University, University Park, Pennsylvania 16802, United States

[⊥]Chemical Sciences and Engineering Division, Argonne National Laboratory, 9700 South Cass Avenue, Argonne, Illinois 60439, United States

Supporting Information

ABSTRACT: Supported nickel catalysts are widely used in hydrocarbon steam reforming for producing hydrogen. Carbon deposition is a major cause of Ni catalyst deactivation. In this work, supported Ni and Ni/Rh catalysts were synthesized and tested for liquid hydrocarbon steam reforming. Carbon analysis on the spent catalysts illustrates that the carbon deposition is significantly reduced with inclusion of Rh. Extended X-ray Absorption Fine Structure (EXAFS) analysis indicates close interactions between Ni and Rh atoms. Density functional theory (DFT) results show that a Ni/Rh alloy is thermodynamically more stable than Ni and Rh alone at the synthesis and reaction temperatures. Adsorption, diffusion, and oxidation of carbon atoms over Ni and Ni/Rh alloy surfaces were examined by DFT calculations. Alloying with Rh reduces the stability of deposited carbon atoms and clusters over both terraces and steps of the catalyst. Moreover, Rh addition enhances the competition of oxidation reactions against carbon deposition by altering the relative diffusion rates and bond formation rates of the two processes.

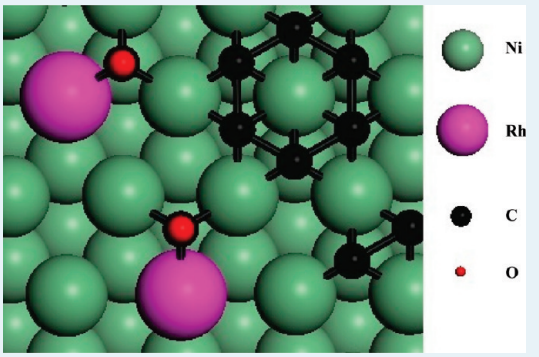

KEYWORDS: steam reforming, deactivation, coking, nickel, rhodium, Ni−Rh, catalyst, DFT, stepped surfaces, reforming, EXAFS

1. INTRODUCTION

Hydrogen (H_2) is an important reactant for industrial chemical synthesis and petroleum refining. Hydrogen is also proposed as a major energy carrier for an efficient, sustainable energy infrastructure because the energy stored in hydrogen can be efficiently used to generate electricity in fuel cells. The most widely used industrial method for H_2 production is hydrocarbon steam reforming over Ni-based catalysts. However, under the low O/C ratios optimal for overall energy efficiency, Ni catalysts deactivate because of carbon deposition.[1−4] Binary metal catalysts could be more carbon resistant compared with the monometallic Ni catalyst,[5−9] because the addition of the second metal changes the surface composition, which may affect the carbon chemistry over the catalyst surface. Bimetallic Ni/Rh catalysts were reported to be sulfur tolerant during reforming of model jet fuel in our previous experimental work.[10] Herein, we study the carbon resistance of Ni/Rh catalysts during liquid hydrocarbon steam reforming and apply density functional theory (DFT) to investigate elementary reaction energetics to explain the modifications induced by Rh inclusion.

In the reforming process over Ni catalysts, carbon deposition occurs via either hydrocarbon decomposition ($C_nH_{2n+2} \rightarrow nC + (n+1)H_2$) or CO disproportionation ($2CO \rightarrow CO_2 + C$) reactions.[2−4] For on-board hydrogen production for fuel cell systems, liquid hydrocarbons attract more interest than gaseous feedstock such as natural gas because of the higher energy density and easier storage of liquid fuels.[11] However, the use of heavier hydrocarbons can cause more severe carbon deposition,[11,12] which can encapsulate the Ni surface or diffuse through Ni particles to generate whisker carbon that contaminates the catalysts and plugs reactor flow channels.[3,9,13] At the molecular scale, the initial stages of deposited carbons are surface bound carbon clusters, graphene islands, or inclusion of C atoms into subsurface sites toward a carbide-like structure.[14] Carbon covered surfaces or bulk carbides no longer catalyze the reforming reaction because active Ni sites are blocked.

Received: January 31, 2011
Revised: March 27, 2011
Published: March 30, 2011

Numerous studies have tested catalyst formulation changes to enhance the carbon resistance of Ni catalysts. Sulfur addition was reported[3,7] to suppress carbon deposition by selectively blocking the most active sites for carbon nucleation; however, sulfur also poisons the catalyst. A binary Ni/Au catalyst was carbon resistant compared with the monometallic Ni catalyst,[5,15] but Au decreases the overall catalyst activity because of less effective C−H bond activation.[5,16,17] Ni/Sn was reported to be carbon tolerant by experimental studies.[9,18−21] DFT studies[8,9] showed that Ni/Sn inhibits carbon deactivation by slowing C−C bond formation. But DFT results have also shown that the energy barrier to CH_4 activation over Ni/Sn(111) is slightly higher than that over Ni(111).[22] Addition of a small amount of boron was found to decrease the stabilities of bulk carbide and surface graphene islands,[14,23,24] which thereby protects the catalyst from coking. However, it is unclear from the literature[24,25] whether the inclusion of B leads to an increase in CH_4 activation barrier.

Noble metals such as Rh show better coking resistance and reforming activity than Ni,[2,26−28] but monometallic Rh catalysts are more expensive and are prone to poisoning by sulfur compounds in the fuel. A Ni/Rh bimetallic catalyst was reported to be more sulfur tolerant and more active than a monometallic Rh catalyst.[10,29−32] Studies using Ni/Rh catalysts for steam reforming of methane,[33] *n*-butane,[34] and *n*-hexadecane[35] also suggested Ni/Rh is more carbon resistant than supported Ni catalysts. In the present study, supported Ni and Ni/Rh catalysts were synthesized and tested for steam reforming of Norpar13 (a model fuel of jet fuel from Exxon Mobil comprising mainly C12−C14 normal paraffins with an average carbon number of 13). Carbon analysis on the spent catalysts illustrates that the carbon deposition is significantly reduced in the presence of Rh. Extended X-ray Absorption Fine Structure (EXAFS) and computational results indicate that Rh−Ni forms an alloy. To provide insight into the mechanistic changes introduced by Rh, carbon diffusion, C−C formation, and carbon oxidation energetics over Ni and Ni/Rh alloy surfaces were examined using DFT calculations.

2. METHODS

2.1. Experimental Section. CeO_2-modified Al_2O_3 (CeAl) support with 20 wt % of CeO_2 loading was prepared by wet-impregnation of $Ce(NO_3)_3$ (Aldrich) onto γ-Al_2O_3 (PURALOX TH 100/150, Sasol, BET: ∼150 m^2/g). It was found that the addition of ceria to alumina promotes the reforming of liquid and gaseous fuels.[10,29,36,37] The mixture solution was dried overnight, followed by calcination at 550 °C. The supported Ni catalyst was prepared by wet impregnation of $Ni(NO_3)_2$ (Aldrich) onto the CeAl support at a 10 wt % of Ni loading. Previous work[10] has illustrated that 10 wt %Ni-2 wt %Rh/CeO_2−Al_2O_3 was most resistant to deactivation and had high activity among *x*Ni-2 wt % Rh/CeO_2−Al_2O_3 (*x* = 0, 2, 5, 10, and 20 wt %) catalysts for steam reforming of liquid hydrocarbon fuels at 520 °C. Therefore, the present study focuses on the 10 wt %Ni-2 wt %Rh/CeO_2−Al_2O_3 catalyst with Rh/Ni atomic ratio of 1:8.8. For the bimetallic catalyst, the metals were loaded by co-impregnation of $Ni(NO_3)_2$ and $Rh(NO_3)_3$ onto the same support at 2 and 10 wt % for Rh and Ni, respectively. The basic physical properties of the monometallic Ni and bimetallic Ni−Rh catalysts have been reported in a previous study.[38] As a brief summary, the textural properties of the two catalysts are presented here: 109 m^2/g (BET surface area) and 0.54 cm^3/g (pore volume) for Ni/CeAl, and 102 m^2/g (BET surface area) and 0.49 cm^3/g (pore volume) for Ni−Rh/CeAl.

The thus-obtained catalysts were dried overnight, followed by calcination at 550 °C. Steam reforming of sulfur-free Norpar13 (Normal paraffin content: >99 wt % with a small amount of other types of hydrocarbons such as aromatics) was conducted at 550 °C and 1 atm with a steam-to-carbon molar ratio of 3.0 and a WHSV of 5.1 h^{-1}. To study the deposited carbon species over the spent catalysts, temperature programmed oxidation (TPO) was performed using a LECO RC-412 multiphase carbon analyzer. The sample was heated from ambient temperature to 900 °C at a rate of 30 °C/min in UHP oxygen.

2.2. EXAFS. X-ray absorption measurements were made on the 10BM beamline of the Materials Research Collaborative Access Team (MRCAT) at the Advanced Photon Source, Argonne National Laboratory. The beam was detuned to 50% of the maximum intensity to minimize the presence of harmonics. Measurements were made in step scan mode at 0.2 s per point in transmission mode with the ionization chambers optimized for the maximum current with linear response (∼10^{10} photons detected/s) using a mixture of nitrogen and helium in the incident X-ray detector and a mixture of about 50% argon in nitrogen in the transmission X-ray detector. A nickel foil spectrum was acquired simultaneously with each measurement for energy calibration.

Dried catalyst samples were pressed into a cylindrical holder with a thickness chosen to give a total absorbance (μx), at the Rh*K* (24.220 keV) edge and Ni*K* (8.333 keV), of about 2.0 and an edge step ($\Delta\mu x$) of about 0.5−1.0. The catalysts were treated in a continuous-flow EXAFS reactor cell (18 in. long, 0.75 in diam.) fitted at both ends with polyimide windows and valves to isolate the reactor from the atmosphere. The spectra were obtained at room temperature. The monometallic Rh and binary Rh−Ni catalysts were analyzed as received and reduced at 550 °C for 60 min in 4% H_2/He. EXAFS results were fitted using Artemis with FEFF8. EXAFS spectra of Ni foil, NiO, Rh foil, Rh_2O_3 were recorded at room temperature as the references for the EXAFS fitting.

2.3. Computational Methods. Periodic, spin-polarized density functional theory (DFT) calculations were carried out using the Vienna Ab-initio Simulation Program (VASP), an ab initio total-energy and molecular dynamics program developed at the Institute for Material Physics at the University of Vienna.[39−41] The projector augmented wave (PAW) method[42] was used to represent the wave functions of core electrons. The wave functions of valence electrons were described with plane wave basis sets and were limited by a cutoff energy of 400 eV. The valence configurations for nickel are $3d^8 4s^2$, for rhodium $4d^8 5s^1$, for carbon $2s^2 2p^2$, for oxygen $2s^2 2p^4$ and for hydrogen $1s^1$. The Perdew−Wang 91 (PW91) form of the generalized gradient approximation (GGA) was used for exchange and correlation energies.[43] The Brillouin zone was sampled using a 13 × 13 × 13 Monkhorst−Pack (MP)[44] k-point mesh for bulk Ni and bulk Rh, a 5 × 5 × 5 MP k-point mesh for bulk alloy Ni_2Rh_1, and a 3 × 3 × 1 MP k-point mesh for surfaces. The electronic self-consistent field was converged to 1 × 10^{-4} eV, and the structural optimization was continued until the forces on all atoms were less than 0.05 eV/Å. The spurious slab-to-slab dipole interaction was validated to be substantially small (<0.003 eV) by comparing the energies calculated with and without a dipole correction, which includes corrections for surface normal dipole−dipole interactions within the electronic self-consistent field cycle.

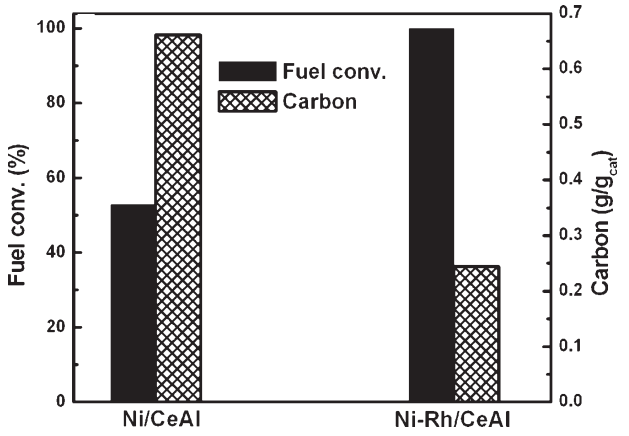

Figure 1. Amounts of carbon deposits and fuel conversions for steam reforming of Norpar13 over 10 wt %Ni/CeO_2−Al_2O_3 and 10 wt %Ni-2 wt %Rh/CeO_2−Al_2O_3 after 55 h on stream (the fuel conversions were measured at 55 h TOS).

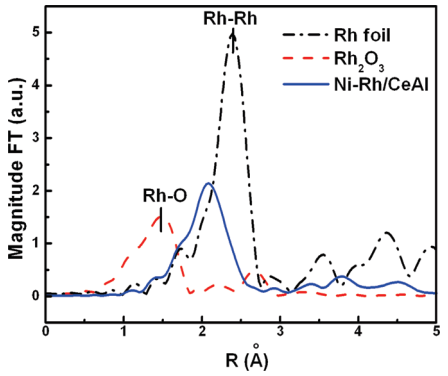

Figure 2. Fourier transform Rh K-edge EXAFS of Rh references (Rh foil and Rh_2O_3 used as received without any pretreatment) and 10 wt % Ni-2 wt %Rh/CeO_2−Al_2O_3 (10Ni2Rh/CeAl) (k^2: Δk = 2−14 $Å^{-1}$). The bimetallic catalyst was reduced at 550 °C for 60 min in 4% H_2/He prior to EXAFS analysis.

Zero point vibrational energy (ZPVE) corrections were included in the adsorption energies and activation barriers. ZPVE was determined by harmonic vibrational frequency calculations, in which the Hessian matrix was only constructed with second derivatives of energy with respect to position of the adsorbate atoms. Transition states were located for key steps in carbon deposition and carbon oxidation using the climbing image nudged elastic band method (NEB-CI).[45−47] Within the method, a series of images along the path of the reactants and the products are generated and optimized, with constraints to remain spaced along the reaction coordinate. A transition state is identified as the image with the highest energy, an absolute force tangential to the reaction coordinate of less than 0.05 eV/Å, and all atom forces less than 0.05 eV/Å.

Adsorption and reaction were considered on (111) and (211) surfaces, representing terrace and step sites, respectively. The (111) surface is the most stable surface of Ni and Rh, whereas the (211) step surface is more active for C−H and C−C dissociation reactions.[22,48] For the (111) surface, a 4-layer, 3 × 3 supercell slab with the top two layers fully relaxed was used. A vacuum region equal to six metal layers separated the slabs in the direction perpendicular to the surface. The (211) surface was modeled with a 3 × 1 surface cell and a 9-layer thick slab with the top four layers relaxed. An eighteen-layer vacuum was built above the surface. The slab size, vacuum spacing, and structural convergence criteria were confirmed to converge the total energy to within 0.03 eV. The k-point sampling was confirmed to converge the calculated adsorption energy to within 0.03 eV. The specific Ni/Rh alloy surface structures are described individually with the presentation of results.

3. RESULTS

3.1. Carbon Content on Used Catalysts. Figure 1 compares the carbon contents on the spent Ni and Ni/Rh catalysts after steam reforming of Norpar13 at 550 °C for 55 h. TPO results showed that 0.66 g/g_{cat} of carbon species were deposited on the Ni catalyst, which was reduced to 0.24 g/g_{cat} with the Rh addition. The same beneficial effect of Rh on the reduced carbon formation on Ni-based reforming catalysts has also been reported by Strohm et al.[10] Their study clearly showed the suppressed carbon deposition on bimetallic Ni−Rh catalysts with different Ni loadings (e.g., 5 and 10 wt %) in steam reforming of Norpar13 fuel. The remarkably different carbon deposition on these two catalysts, along with Strohm et al.'s work,[10] illustrates that the binary Ni/Rh catalyst is more carbon-resistant compared with Ni alone. This distinction can account for the higher fuel conversion of the Ni/Rh catalyst (100%) than that of the Ni catalyst (52.9%) upon Norpar13 reforming with 55 h on stream, as demonstrated in Figure 1 as well. The severe carbon deposition on the Ni catalyst may significantly cover its catalytic reaction sites, giving rise to the lower fuel conversion in the hydrocarbon reforming reaction. The TPO profiles of the used Ni and Ni−Rh catalysts are shown in Supporting Information, Figure S1. They both showed a peak of carbon oxidation in a temperature range from 500 and 600 °C due most likely to the burning off of filamental carbons.[37] Their very similar TPO profiles imply that the addition of Rh did not remarkably affect the reactivity of carbon deposits, though its presence effectively reduced the carbon accumulation on Ni.

3.2. EXAFS Results. Figure 2 shows the Fourier transform Rh K-edge EXAFS of 10Ni2Rh/CeAl and Rh references (Rh foil and Rh_2O_3). The Rh EXAFS of 10Ni2Rh/CeAl is significantly different from those of Rh foil and Rh_2O_3. The Rh peak position notably shifts to lower R in the 10Ni2Rh/CeAl catalyst as compared with that in the Rh foil. This indicates close Ni−Rh interaction in the bimetallic catalyst as suggested by Strohm et al.[10]

Fitting results of Rh K-edge and Ni K-edge EXAFS are summarized in Table 1. A single Rh atom in 10Ni2Rh/CeAl is surrounded by about 6 Ni neighbors and 3 Rh neighbors. Therefore, this result indicates the formation of Ni−Rh alloy in the binary catalyst upon H_2 reduction at 550 °C. Since both Ni and Rh are of FCC structure, the coordination number of Rh should be 12 and 9 when it exists in Ni bulk and on Ni surface, respectively. On the basis of our fitting results (Table 1), the total coordination number of Rh is around 8.8 (sum of 5.8 and 3.0 for Rh−Ni and Rh−Rh at Rh K-edge, respectively), which is very close to 9. This result strongly suggests that Rh atoms prefer to stay on Ni surfaces to form surface Ni−Rh alloy, rather than dissolving into Ni particles to form bulk alloy. Fitting of the Ni EXAFS only indicated the contributions from Ni−O and Ni−Ni bonds, and showed no clear evidence of alloy formation. This is very likely because of the high Ni/Rh molar ratio such that the

dx.doi.org/10.1021/cs2000472 |ACS Catal. 2011, 1, 574–582

Table 1. Fitting Results of Rh K-Edge and Ni K-Edge EXAFS

sample	backscatter	CN	R (Å)	DWF (10^3)	E_0 (eV)
		Rh K-edge			
10Ni2Rh/CeAl[a]	Rh−Ni	5.8 ± 0.5	2.52 ± 0.02	5 ± 0.9	2.5 ± 0.8
	Rh−Rh	3.0 ± 0.6	2.65 ± 0.02	9 ± 3	2.5 ± 0.8
Rh foil[b]	Rh−Rh	12	2.69		
Rh_2O_3[b]	Rh−O	6	2.01		
		Ni K-edge			
10Ni2Rh/CeAl[a]	Ni−Ni	7.2 ± 0.5	2.47 ± 0.02	7 ± 0.5	3.1 ± 0.7
	Ni−O	0.6 ± 0.4	1.98 ± 0.04	7 ± 1.1	3.1 ± 0.7

[a] Pretreatment conditions: 4% H_2/He at 550 and 700 °C for Rh and Ni edge for 1 h, respectively. [b] Used as received without any pretreatment.

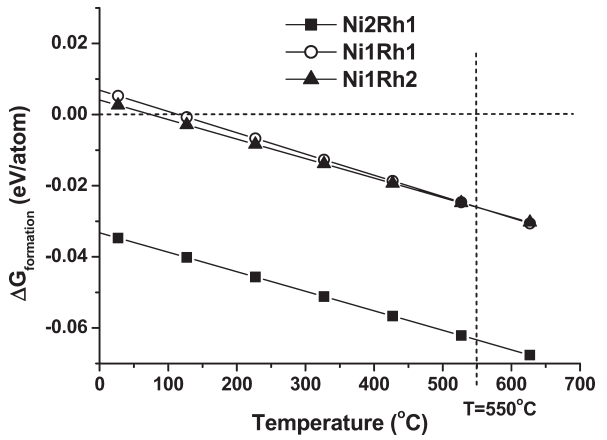

Figure 3. Gibbs free energies of formation of alloys with different Ni/Rh ratios. At the reaction temperature, all the alloys are thermodynamically preferred [$\Delta G(823\ \mathrm{K}) < 0$] with respect to separate Ni and Rh phases.

Ni−Rh contribution is much lower than those of Ni−O and Ni−Ni. In fact, several previous studies[49−51] have indicated that the formation of Ni−Rh bonds in bimetallic Ni−Rh catalysts with high Ni/Rh ratios was hardly observed from Ni K-edge EXAFS.

3.3. Computational Analysis of Stability of Ni/Rh Alloy. The bulk alloy phase diagram[52] suggests a Ni/Rh alloy should be thermodynamically stable relative to separated Ni and Rh phases at the calcination and reaction temperature (550 °C). We performed DFT to calculate the formation energies of Ni/Rh alloys with various Ni:Rh ratios to find a stable bulk model of Ni/Rh alloy for surface calculations. The formation energy per alloy atom was calculated with respect to pure Ni and pure Rh bulk metals as follows:

$$\Delta E_{\mathrm{formation}} = \frac{1}{N(\mathrm{Ni}) + N(\mathrm{Rh})}[(E(\mathrm{alloy}) - N(\mathrm{Ni})\mu(\mathrm{Ni}) - N(\mathrm{Rh})\mu(\mathrm{Rh})] \quad (1)$$

where N(Ni) and N(Rh) are the number of Ni and Rh atoms in the alloy; E(alloy) is the calculated electronic energy of the alloy; μ(Ni) and μ(Rh) correspond to the calculated chemical potential of bulk Ni and Rh, respectively. The entropy per metal alloy is obtained assuming an ideal mixture using the atomic concentration of each metal:

$$\Delta S = -(x_{\mathrm{Ni}} \ln x_{\mathrm{Ni}} + x_{\mathrm{Rh}} \ln x_{\mathrm{Rh}})R \quad (2)$$

The Gibbs free energy per atom of alloy formation at temperature T is calculated as

$$\Delta G_{\mathrm{formation}} = \Delta E_{\mathrm{formation}} - T\Delta S \quad (3)$$

A negative $\Delta G_{\mathrm{formation}}$ indicates the formation of the alloy is thermodynamically stable relative to separated pure metal phases at the corresponding temperature. This simplified approach neglects differences in heat capacity (phonon modes and electronic excitations) between the pure and binary metals. Figure 3 plots $\Delta G_{\mathrm{formation}}$ of Ni_2Rh_1, Ni_1Rh_1, and Ni_1Rh_2 alloys as a function of temperature. At 550 °C, $\Delta G_{\mathrm{formation}} < 0$ for all three Ni/Rh alloys, among which Ni_2Rh_1 is the most stable. The configuration of Ni_2Rh_1 alloy is shown in Figure 4a. The average distance between two metal atoms is 2.59 Å.

To represent a Ni/Rh alloy with low concentration of Rh, we examined the substitutional doping of a single Rh atom into Ni(111) and (211) surfaces. Rh is 0.21 eV (1 eV = 96.48 kJ/mol) and 0.16 eV more stable when substituted in the Ni surface layer than in a subsurface layer for (111) and (211) surfaces, respectively, in agreement with previous DFT studies that indicate surface segregation of Rh.[53] DFT studies have also shown a preference for formation of a mixed Ni−Rh overlayer as opposed to a pure Rh surface.[54] The presence of surface adsorbates could alter these trends; however, the 0.07 eV preference of C to bind to a Ni_3 hollow site over a Ni_2Rh hollow site on the Ni_8Rh/Ni(111) surface is not sufficient enough to alter the segregation preference.

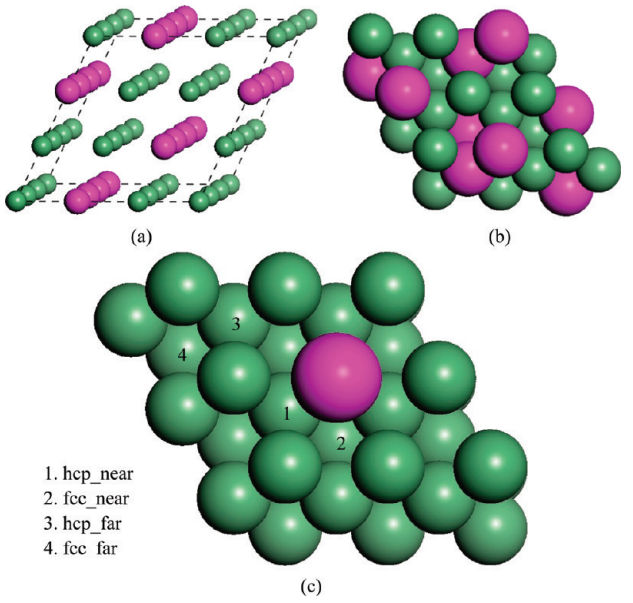

Figure 4. (a) Bulk Ni_2Rh_1 alloy. (b) Top view of Ni_2Rh_1(111) slab. (c) Top view of Ni_8Rh_1/Ni(111) slab. Green (light) spheres represent Ni atoms and purple (dark) spheres represent Rh atoms.

3.4. Computational Studies of Single C or O Atom Diffusion over (111) Surfaces. The elementary reactions of C and O movement over the (111) surfaces were examined using DFT calculations. Chemisorbed C atoms are produced by either hydrocarbon decomposition or CO disproportionation reactions.[7,55] Isolated, adsorbed C atoms can either react with each other to form extended islands of graphene,[56,57] or dissolve into the Ni

dx.doi.org/10.1021/cs2000472 |ACS Catal. 2011, 1, 574–582

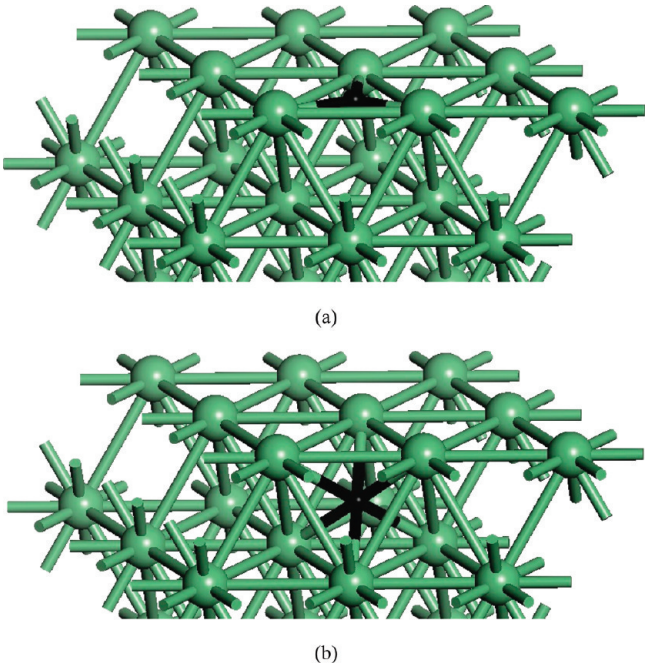

Figure 5. (a) Transition and (b) product states of the diffusion of one C atom from an fcc hollow site to a sublayer octahedral site of the Ni(111) surface. Green (light) spheres represent Ni atoms and black (dark) spheres represent C atoms.

bulk to form carbide species,[58−60] which further leads to the growth of carbon nanotubes.[48,61] The C atoms can be removed from the catalyst surface through oxidation to form CO and CO_2.[8] Solid carbon deposition is avoided if C diffusion and C−C formation are inhibited, or oxidation processes are enhanced. The related elementary steps were examined over Ni and Ni/Rh surfaces. The movement of single C or O atoms and the formation of C−C and C−O bonds over (111) surfaces are examined in sections 3.4 and 3.5, respectively. The stability of deposited carbon was studied by evaluating the adsorption energies of a C atom and a group of 6 C atoms over the (111) terrace and (211) step surfaces in section 3.6.

Four types of Ni/Rh fcc-based structures were investigated for the (111) surface: (1) pure Ni(111); (2) Ni/Rh surface alloy where one Ni atom on the 3 × 3 surface was substituted by a Rh atom, designated Ni_8Rh_1/Ni(111); (3) the (111) surface of Ni/Rh bulk alloy with ratio of Ni/Rh = 2:1, designated Ni_2Rh_1(111) and shown in Figure 4b, and (4) pure Rh(111). Ni_8Rh_1/Ni(111) is a model for a Ni/Rh alloy formed by the surface segregation of a small amount of Rh within a majority Ni alloy. The cell dimensions are set to the substrate Ni bulk lattice vectors. For this model surface, multiple adsorption sites with varying proximity to the surface Rh atom were considered, as labeled in Figure 4c. Ni_2Rh_1(111) uses the lattice vectors optimized for the Ni_2Rh_1 alloy, representing the (111) termination of the bulk alloy.

C atom diffusion on each surface is first examined. Hcp and fcc hollow sites are the two most stable adsorption sites for isolated C atoms chemisorbed over Ni(111).[14,62] Carbon may migrate on the surface between hollow sites or diffuse into the Ni bulk.[14] The barriers to diffusion of C from hcp to fcc and from fcc to sublayer were calculated. The transition state for the hcp-to-fcc movement corresponds to the configuration where C is adsorbed at the bridge site, which is above the midpoint of two neighboring surface metal atoms. For C diffusion from fcc to the sublayer toward formation of the nickel carbide species, the transition and final states are shown in Figure 5.

Table 2. Calculated Reaction Energies and Activation Energies for the Diffusion of Single C Atom from hcp Hollow Site to fcc Hollow Site and from fcc Hollow Site to Sub-Layer Octahedral Site over (111) Surfaces

	from hcp to fcc			from fcc to sublayer		
	reaction energy (eV)	activation energy (eV)	relative rate[a]	reaction energy (eV)	activation energy (eV)	relative rate[a]
Ni(111)	0.06	0.32	1.0	−0.60	0.81	1.0
Ni_8Rh_1/Ni(111)_near	0.10	0.54	0.045	−0.40	1.19	0.0047
Ni_8Rh_1/Ni(111)_far	−0.03	0.25	2.7	−0.59	0.98	0.091
Ni_2Rh_1(111)	0.15	0.40	0.32	−0.38	0.74	27
Rh(111)	0.19	0.69	0.0054	0.16	0.92	0.21

[a] At a temperature of 550 °C.

Table 2 compares the reaction energies, activation energies, and relative reaction rates of the two diffusion steps on the four (111) surfaces. The relative reaction rates were calculated based on the Arrhenius equation as:

$$r = e^{-(E_{TS} - E'_{TS})/RT} \quad (4)$$

where E_{TS} is the activation energy over a particular (111) surface, E'_{TS} is the activation energy over the Ni(111) surface; and the experimental reaction temperature of 823 K was used.

For diffusion of C atoms on the Ni_8Rh_1(111) surface, initial adsorption in two hollow sites was considered: the Ni_2Rh_1 hollow site denoted Ni_8Rh_1/Ni(111)_near, and the Ni_3 hollow site denoted Ni_8Rh_1/Ni(111)_far. The diffusion of one C atom from hcp to fcc is an endothermic process over most of the surface sites studied. Ni(111) and Ni_8Rh_1/Ni(111)_far, which are the two hollow surface sites without a Rh atom, have the lowest energy barriers for surface carbon diffusion. The energy barrier on Ni(111) is 0.26 eV if considering carbon diffusion from the less stable fcc site to the more stable hcp site, very close to that on Ni_8Rh_1/Ni(111)_far (0.25 eV). The addition of Rh to the catalyst slows C diffusion on the neighboring sites of Rh. On the basis of the calculated relative ratio, by introducing Rh into Ni to form Ni_8Rh_1/Ni(111) surface alloy, the C movement from hcp to fcc would be slowed by more than 20 times at 550 °C.

Among the surfaces studied, Ni(111) has the strongest driving force for C to be bonded at the subsurface octahedral site with six neighboring metal atoms. The activation energy of C dissolving into Ni(111) is 0.38 eV lower than that into Ni_8Rh_1/Ni(111) starting from the Ni_2Rh_1 site. Since the reforming experiment was operated at the temperature of 550 °C, a 0.38 eV increase in energy barrier causes carbon diffusion into the sublayer of catalyst to be more than 200 times slower. For C starting at the surface Ni_3 site of Ni_8Rh_1/Ni(111), the reaction energy for C to move to subsurface is similar to that for Ni(111), but the energy barrier is 0.17 eV higher. For Ni_2Rh_1(111), the calculated barrier is lower than that of Ni(111); however, the reduced driving force for the overall reaction may lead to less subsurface carbon. C adsorbed to Ni(111) more easily dissolves into the sublayer to form the stable

dx.doi.org/10.1021/cs2000472 |ACS Catal. 2011, 1, 574–582

Table 3. Calculated Activation Energies and Reaction Energies for the Diffusion of Single O Atom from hcp Hollow Site to fcc Hollow Site

	reaction energy (eV)	activation energy (eV)	relative rate[a]
Ni(111)	−0.12	0.38	1.0
Ni_8Rh_1/Ni(111)_near	−0.11	0.43	0.49
Ni_8Rh_1/Ni(111)_far	−0.17	0.37	1.2
Ni_2Rh_1(111)	−0.01	0.29	3.6
Rh(111)	−0.06	0.39	0.87

[a] At a temperature of 550 °C.

nickel carbide, whereas Rh alloyed Ni(111) inhibits this process by decreasing the driving force and slowing down the reaction rate.

The hcp-bridge-fcc diffusion of a chemisorbed O atom over (111) surfaces was also examined, with results reported in Table 3. Comparing Ni(111) with Ni_8Rh_1/Ni(111), the activation energy of O diffusion about the Rh atom is increased by only 0.05 eV (from 0.38 to 0.43 eV); whereas it varies little at sites further from the Rh atom (from 0.38 to 0.37 eV). Compared to the energy barrier change of carbon diffusion due to Rh addition (0.22 eV increase), the impact of Rh on the O diffusion rate is much less. Moreover, the bulk alloy surface Ni_2Rh_1(111) shows an even lower energy barrier (0.29 eV) for O moving from hcp to fcc. The trends of Rh increasing the C diffusion barrier while having a minimal effect or reducing the O diffusion barrier are equivalent for the reverse process, that is, diffusion from fcc to hcp.

3.5. Computational Studies of C−C and C−O Formation over (111) Surfaces. C atoms on the Ni surface could form graphenic carbon, which blocks the surface active sites.[56,57] The initial formation energetics were calculated to examine the impact of Rh addition on carbon bond formation, similar to previous studies of Ni/Sn systems by the Linic group.[8,9] As the initial state, two C atoms are adsorbed at two neighboring hcp hollow sites. One C atom overcomes an energy barrier and diffuses to the neighboring fcc hollow site, forming a C−C bond with the other C atom remaining at an hcp site. This reaction is illustrated in Figure 6.

The calculated reaction energies and activation barriers are given in Table 4. The C−C bond formation energy was calculated as the difference in adsorption energies by comparing C−C adsorbed together over neighboring hcp and fcc sites to two C atoms individually adsorbed over hcp and fcc sites:

$$E_b = \Delta E_{ads}(C - C^*) - \Delta E_{ads}(C^*_{hcp}) - \Delta E_{ads}(C^*_{fcc}) \quad (5)$$

where $\Delta E_{ads}(C-C^*)$, $\Delta E_{ads}(C^*_{hcp})$, and $\Delta E_{ads}(C^*_{fcc})$ could be obtained as:

$$\Delta E_{ads}(C - C^*) = E_{C-C^*} - E_{slab} - 2E_C \quad (6)$$

$$\Delta E_{ads}(C^*) = E_{C^*} - E_{slab} - E_C \quad (7)$$

E_{C-C^*}, E_{C^*}, E_{slab}, and E_C represent the total DFT energy of the combined C−C/slab system, C/slab system, the clean surface slab, and the free C atom. This bond formation energy differs from the reaction energy by the interaction energy between the two adjacent bound C prior to C−C bond formation. On the basis of the results in Table 4, the C−C formation process over Ni(111) is more exothermic and has a lower activation barrier than the Rh-containing (111) surfaces. Therefore, the addition of

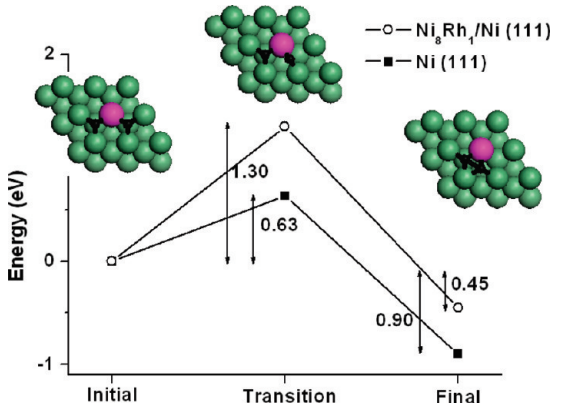

Figure 6. Top views of the C−C formation reaction over Ni_8Rh_1/Ni(111), and relative energies of initial, transition, and final states of C−C formation over Ni(111) and Ni_8Rh_1/Ni (111). Green (light) spheres represent Ni atoms, purple (dark large) spheres represent Rh atoms, black (dark small) represent C atoms.

Table 4. Calculated Activation Energies and Reaction Energies for C−C Formation over (111) Surfaces

	reaction energy (eV)	E_b[a] (eV)	activation energy (eV)	relative rate[b]
Ni(111)	−0.90	−0.50	0.63	1.0
Ni_8Rh_1/Ni(111)_near	−0.45	−0.21	1.30	0.000078
Ni_8Rh_1/Ni(111)_far	−0.68	−0.65	1.31	0.000069
Ni_2Rh_1(111)	−0.69	−0.32	0.75	0.18
Rh(111)	0.19	0.24	1.34	0.000045

[a] As shown in eq (5). [b] At a temperature of 550 °C.

Rh on Ni surface inhibits the C−C formation process both thermodynamically and kinetically.

C atoms are removed from the reforming catalyst surface by oxidation reactions. The oxidation process converting adsorbed C and O atoms to CO was examined. The transition state for C−O formation is located from an initial configuration where one C atom and one O atom are adsorbed over neighboring hcp sites.[8] Nikolla et al.[8,9] have shown the highest barrier to C−O formation occurs for the final O diffusion from a nearby hollow site. In the final state, CO adsorbs through the C atom with its bond axis perpendicular to the surface plane. The calculated energies are listed in Table 5, and Figure 7 illustrates the reaction energy diagram for this reaction. The barrier for the reverse reaction of C−O dissociation on the Ni(111) surface (2.99 eV) is close to the value of 2.85 eV reported by a previous computational study using similar methods.[63] The introduction of a Rh atom to the Ni surface increases the energy barrier of CO formation by 0.23 eV (from 1.18 to 1.41 eV), which is not as significant as the energy barrier change of C−C formation due to Rh addition (0.67 eV). In the case of Ni_2Rh_1(111), the energy barrier of CO formation is lower than that of Ni(111). The addition of Rh to the surface therefore slows C−C bond formation whereas C−O formation is less affected or even promoted.

3.6. Computational Studies of Adsorption Energies of C-6 over (111) and (211) Surfaces. The steps of reforming catalysts

dx.doi.org/10.1021/cs2000472 |ACS Catal. 2011, 1, 574–582

Table 5. Calculated Activation Energies and Reaction Energies for the C−O Formation over (111) Surfaces

	reaction energy (eV)	activation energy (eV)	relative rate[a]
Ni(111)	−1.75	1.18	1.0
Ni_8Rh_1/ Ni(111)_near	−1.83	1.41	0.039
Ni_8Rh_1/Ni(111)_far	−1.72	1.29	0.21
Ni_2Rh_1(111)	−1.66	1.16	1.3
Rh(111)	−1.43	1.37	0.069

[a] At a temperature of 550 °C.

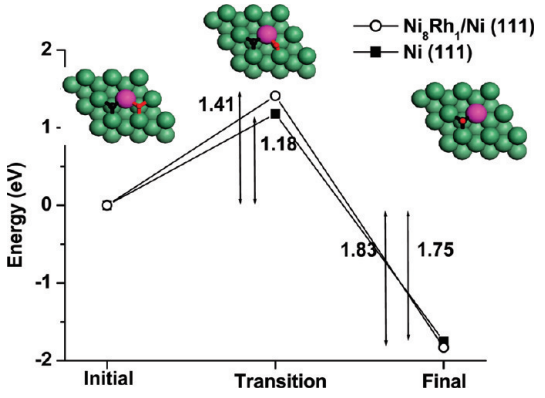

Figure 7. Top views of the C−O formation reaction over Ni_8Rh_1/Ni(111), and relative energies of initial, transition, and final states of C−O formation over Ni(111) and Ni_8Rh_1/Ni(111). Green (light large) spheres represent Ni atoms, purple (dark large) spheres represent Rh atoms, black (dark small) spheres represent C atoms, red (light small) spheres represent O atoms.

are more active for C−C and C−H bond activation than flat surfaces.[22,48] To examine whether Rh addition also protects steps from carbon deposition, the adsorption energies of one C atom and an extended double row of 6 C atoms (C-6) over (211) step surfaces were determined. Three types of surfaces were investigated: (1) pure Ni(211); (2) Ni/Rh surface alloy where one Rh atom substitutes one Ni atom on the 3 × 1 surface, designated $Ni_8Rh_1(211)$; (3) pure Rh(211). The adsorption energy of one C atom was calculated as eq 7, and the adsorption energy of C-6 was calculated as

$$\Delta E_{ads}(C-6^*) = (E_{C-6^*} - E_{slab} - 6E_C)/6 \qquad (8)$$

where E_{C-6^*} represents the total DFT energy of the combined C-6/slab system. The results are compared with the (111) surface and summarized in Table 6. The adsorption configurations of the C-6 over (111) and (211) surfaces are shown in Figure 8. Both single C atoms and C-6 clusters bind weaker over Ni/Rh surfaces than over pure Ni surfaces. For the Ni(111), C-6 clusters are more stable than isolated C atoms, whereas the addition of Rh makes the preference to be opposite.

4. DISCUSSION

Comparison of the carbon contents on the used catalysts, on a per catalyst weight basis, shows that Rh aids the carbon-resistance of Ni/Rh reforming catalysts. Similar results were also shown in the study of dry reforming of methane by comparing

Table 6. Calculated Adsorption Energies of One C Atom and C6-Cluster over Pure Ni Surfaces [Ni(111) and Ni(211)] and Ni/Rh Alloy Surfaces (Ni_8Rh_1/Ni(111) and Ni_8Rh_1/Ni(211))

	(111)		(211)	
E_{ad}/atom (eV)	C atom	C-6 cluster	C atom	C-6 cluster
pure Ni surfaces	−6.74	−6.76	−7.67	−7.53
Ni/Rh alloy surfaces	−6.67	−6.56	−6.93	−6.86
pure Rh surfaces	−7.08	−6.57	n.a.	n.a.

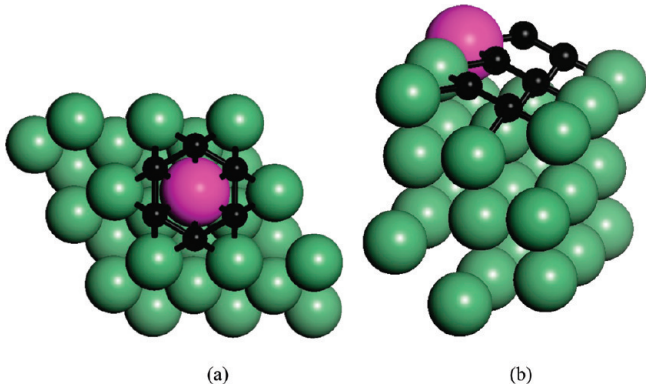

Figure 8. Adsorption configurations of (a) a C-6 cluster over Ni_8Rh_1/Ni(111), top view; (b) an extended double row of 6 C atoms over Ni_8Rh_1/Ni (211), side view. Green (light) spheres represent Ni atoms, purple (dark large) spheres represent Rh atoms, black (dark small) represent C atoms.

the carbon contents over Ni and Ni/Rh. EXAFS results indicate a substantial Rh−Ni coordination number and are consistent with Rh being in the surface of the catalyst, motivating our choice of DFT model surfaces for study.

Thermodynamically, Rh reduces the driving force for single carbon atoms to deposit, for forming C−C bonds and C-6 clusters, and for C dissolution into the catalyst. Kinetically, alloying with Rh dramatically slows down the reaction steps of C diffusion and C−C formation needed for deposition, whereas O diffusion and C−O formation are not affected as significantly or are accelerated to oxidize carbon from the surface. Therefore, Rh addition may enhance the competition of oxidation reactions with carbon deposition by altering the relative surface diffusion rates and bond formation rates of the two processes. Our analysis considered C−C and C−O bond formation occurring among completely dehydrogenated species, though C−C and C−O bonds may form prior to complete dehydrogenation. A subset of calculations were performed to confirm that trends in diffusion barriers held partially hydrogenated species, however, a complete analysis was not performed. Please see Supporting Information for details as to the calculations performed on partially hydrogenated species.

The reduced driving force to carbon species formation over Ni/Rh surfaces may be due to the larger Rh atomic size and the resultant strain in the surface. As shown in Table 6, although isolated C atoms are adsorbed stronger over Rh(111) than Ni(111), they become less stable to form clusters over Rh. The reduced stability of the graphenic cluster on Rh may be due to the larger Rh atomic size than Ni, which makes the distance between each hollow site not match with the C−C bond length of C

dx.doi.org/10.1021/cs2000472 |ACS Catal. 2011, 1, 574–582

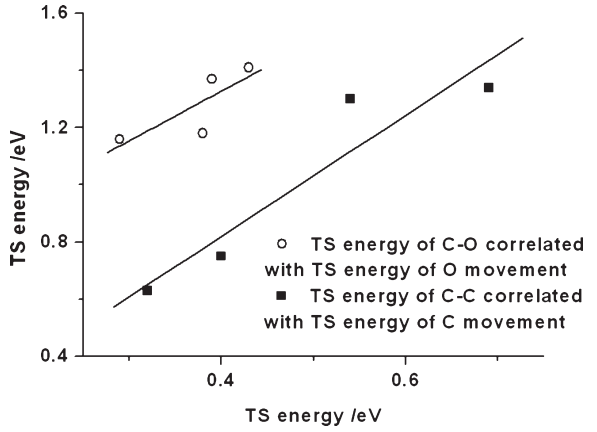

Figure 9. Correlation between transition state energy of C−C formation and transition state energy of C surface diffusion (square solid), and correlation between transition state energy of C−O formation and transition state energy of O movement (circle hollow).

clusters. On the basis of our DFT calculations, the C−C bond distance in a graphite system equals to 1.42 Å, which is closer to the distance between neighboring hollow sites over Ni (1.44 Å for Ni, 1.57 Å for Rh). The larger atomic size of Rh also blocks subsurface C diffusion through the hollow sites in the Ni_8Rh_1/Ni(111) surface by increasing this diffusion barrier. For the Ni_3 site of Ni_8Rh_1/Ni(111), the increase in barrier without direct binding to the surface Rh atoms is likely due to the inclusion of the larger Rh atom in the surface restricting the expansion of the Ni_3 hollow site needed to let the C atom pass from the surface to the subsurface. The adsorption of C on Ni_8Rh_1/Ni(111) is less stable than on both Ni(111) and Rh(111), which might be explained with the computational observation that adsorption energies become weaker over compressively strained metal surfaces.[64]

Differences in C and O single atom bonding to Ni and Rh do not follow the same trend, consistent with the trends in energetics of C and O related diffusion and bond formation. Contrary to the C atom trend, the O atom adsorbs on Rh(111) weaker than on Ni(111). This difference has been previously reported[65] and explained in term of differences in the electronic interactions involved in C and O binding. Van Santen and Neurock[65] showed that the periodic trends in binding of C and O to closed-pack metal surfaces differ substantially, with O forming a polar metal-adsorbate bond that is stronger on metals up and to the left in the d-block, whereas the strength of the more covalent metal-C bond is relatively metal independent.

The activation barriers for C−C formation and C−O formation correlate with those for C and O surface diffusion, as shown in Figure 9. Linear relationships were found for both cases which might be explained by the configurations of initial, transition, and final states shown in Figure 6 and Figure 7, where the formation process of C−C/C-O is mainly a movement process of one C/O atom. As a result, the energy barrier of C−C/C−O formation could be predicted by calculating the energy barrier of single C/O movement over a specific surface, which could save computational time for the transition state search over other metal surfaces.

Although the Ni_2Rh_1(111) model has higher Rh content than Ni_8Rh_1/Ni(111) does, the differences in the lattice dimensions and composition of the subsurface (Ni_2Rh_1 for Ni_2Rh_1(111) model and pure Ni for Ni_8Rh_1(111) model) make electronic properties disproportional to the Rh concentration. As shown in our results, the energy barriers on Ni_2Rh_1(111) are only larger than those on Ni(111), but lower than those on Ni_8Rh_1/Ni(111), suggesting Rh concentration alone does not dictate surface energetics.

The reforming activity of Ni/Rh catalyst is also of interest. Dissociation barriers of C−C, C−H, and C−O should follow similar trends over different surfaces.[66] As C−C bond dissociation is the reverse reaction step of C−C formation, the activation barrier of C−C dissociation could also be calculated based on the results in Table 4. The energy barrier of C−C dissociation over Ni_2Rh_1(111) is found to be 1.44 eV, lower than that over pure Ni(111) (1.53 eV). Among the four surfaces studied, pure Rh(111) should be most active in reforming because it has the lowest energy barrier for C−C dissociation (1.15 eV).

5. CONCLUSIONS

A Ni/Rh bimetallic catalyst was synthesized and tested in the steam reforming of liquid hydrocarbons. The deactivation behavior and carbon deposition amount show that the Ni/Rh catalyst is more carbon resistant than a monometallic Ni catalyst. EXAFS analysis showed Ni−Rh interactions, and DFT calculations corroborated the stability of Ni/Rh alloys. The presence of Rh increases the energy barriers of C diffusion and C−C bond formation, thus slowing down both graphene and metal carbide formation; whereas O diffusion and C−O bond formation are not significantly affected. The Rh alloy also reduces the stability of deposited carbon over both terraces and steps of the catalyst.

■ ASSOCIATED CONTENT

Ⓢ Supporting Information. Activation energies and reaction energies for the oxidation of hydrogenated carbon (CH−O formation) over (111) surfaces. This material is available free of charge via the Internet at http://pubs.acs.org.

■ AUTHOR INFORMATION

Corresponding Author

*E-mail: csong@psu.edu (C.S.S.), mjanik@psu.edu (M.J.J.). Phone: 814-863-4466 (C.S.S.), 814-308-3798 (M.J.J.).

■ ACKNOWLEDGMENT

The authors gratefully acknowledge the support of this work in part by the U.S. Department of Energy National Energy Technology Laboratory under Grant DE-NT0004396, by the U.S. Office of Naval Research through an ONR NAVSEA Grant N00014-06-1-0320, and by a fellowship from ConocoPhillips Corp. Use of the Advanced Photon Source was supported by the U.S. Department of Energy, Office of Basic Energy Sciences, Office of Science (DOE-BES-SC), under Contract No. W-31-109-Eng-38. Materials Research Collaborative Access Team (MRCAT) operations are supported by the Department of Energy and the MRCAT member institutions.

■ REFERENCES

(1) In *Catalytic Steam Reforming, Catalysis-Science and Technology*; Rostrup-Nielsen, J. R., Ed.; Springer-Verlag: Berlin, 1984.
(2) Rostrup-Nielsen, J. R. *Catal. Today* **1993**, *18*, 305–324.
(3) Trimm, D. L. *Catal. Today* **1997**, *37*, 233–238.
(4) Trimm, D. L. *Catal. Today* **1999**, *49*, 3–10.

(5) Besenbacher, F.; Chorkendorff, I.; Clausen, B. S.; Hammer, B.; Molenbroek, A. M.; Nørskov, J. K.; Stensgaard, I. *Science* **1998**, *279*, 1913–1915.
(6) Osaki, T.; Mori, T. *J. Catal.* **2001**, *204*, 89–97.
(7) Bengaard, H. S.; Nørskov, J. K.; Sehested, J.; Clausen, B. S.; Nielsen, L. P.; Molenbroek, A. M.; Rostrup-Nielsen, J. R. *J. Catal.* **2002**, *209*, 365–384.
(8) Nikolla, E.; Holewinski, A.; Schwank, J.; Linic, S. *J. Am. Chem. Soc.* **2006**, *128*, 11354–11355.
(9) Nikolla, E.; Schwank, J.; Linic, S. *J. Catal.* **2007**, *250*, 85–93.
(10) Strohm, J. J.; Zheng, J.; Song, C. S. *J. Catal.* **2006**, *238*, 309–320.
(11) Song, C. S. *Catal. Today* **2002**, *77*, 17–49.
(12) Zheng, J.; Strohm, J. J.; Song, C. *Fuel Process. Technol.* **2008**, *89*, 440–448.
(13) Pan, W.; Song, C. S. *Catal. Today* **2009**, *148*, 232–242.
(14) Xu, J.; Saeys, M. *J. Catal.* **2006**, *242*, 217–226.
(15) Molenbroek, A. M.; Nørskov, J. K.; Clausen, B. S. *J. Phys. Chem. B* **2001**, *105*, 5450–5458.
(16) Holmblad, P. M.; Larsen, J. H.; Chorkendorff, I. *J. Chem. Phys.* **1996**, *104*, 7289–7295.
(17) Kratzer, P.; Hammer, B.; Nørskov, J. K. *J. Chem. Phys.* **1996**, *105*, 5595–5604.
(18) Nikolla, E.; Schwank, J.; Linic, S. *J. Electrochem. Soc.* **2009**, *156*, B1312–B1316.
(19) Nikolla, E.; Schwank, J. W.; Linic, S. *Catal. Today* **2008**, *136*, 243–248.
(20) Choi, J. S.; Moon, K. I.; Kim, Y. G.; Lee, J. S.; Kim, C. H.; Trimm, D. L. *Catal. Lett.* **1998**, *52*, 43–47.
(21) Nichio, N.; Casella, M. L.; Santori, G. F.; Ponzi, E. N.; Ferretti, O. A. *Catal. Today* **2000**, *62*, 231–240.
(22) Nikolla, E.; Schwank, J.; Linic, S. *J. Catal.* **2009**, *263*, 220–227.
(23) Xu, J.; Chen, L. W.; Tan, K. F.; Borgna, A.; Saeys, M. *J. Catal.* **2009**, *261*, 158–165.
(24) Xu, J.; Saeys, M. *J. Phys. Chem. C* **2009**, *113*, 4099–4106.
(25) Xu, J.; Saeys, M. *Chem. Eng. Sci.* **2007**, *62*, 5039–5041.
(26) Rostrup-Nielsen, J. R.; Christensen, T. S.; Dybkjaer, I. *Stud. Surf. Sci. Catal.* **1998**, *113*, 81–95.
(27) Chen, Y. S.; Xie, C.; Li, Y.; Song, C. S.; Bolin, T. B. *Phys. Chem. Chem. Phys.* **2010**, *12*, 5707–5711.
(28) Shekhawat, D.; Gardner, T. H.; Berry, D. A.; Salazar, M.; Haynes, D. J.; Spivey, J. J. *Appl. Catal., A* **2006**, *311*, 8–16.
(29) Li, Y.; Wang, X. X.; Xie, C.; Song, C. S. *Appl. Catal., A* **2009**, *357*, 213–222.
(30) Kugai, J.; Velu, S.; Song, C. S. *Catal. Lett.* **2005**, *101*, 255–264.
(31) Kugai, J.; Subramani, V.; Song, C. S.; Engelhard, M. H.; Chin, Y. H. *J. Catal.* **2006**, *238*, 430–440.
(32) Lee, K.; Song, C. S.; Janik, M. J. *Appl. Catal., A* **2010**, *389*, 122–130.
(33) Basile, F.; Fornasari, G.; Trifiro, F.; Vaccari, A. *Catal. Today* **2002**, *77*, 215–223.
(34) Ferrandon, M.; Kropf, A. J.; Krause, T. *Appl. Catal., A* **2010**, *379*, 121–128.
(35) Kim, D. H.; Kang, J. S.; Lee, Y. J.; Park, N. K.; Kim, Y. C.; Hong, S. I.; Moon, D. J. *Catal. Today* **2008**, *136*, 228–234.
(36) Natesakhawat, S.; Oktar, M.; Ozkan, U. S. *J. Mol. Catal. A: Chem.* **2005**, *241*, 133–146.
(37) Natesakhawat, S.; Watson, R. B.; Wang, X. Q.; Ozkan, U. S. *J. Catal.* **2005**, *234*, 496–508.
(38) Xie, C. *Appl. Catal., A* **2010**, *390*, 210.
(39) Kresse, G.; Furthmuller, J. *Comput. Mater. Sci.* **1996**, *6*, 15–50.
(40) Kresse, G.; Hafner, J. *Phys. Rev. B* **1993**, *47*, 558–561.
(41) Kresse, G.; Furthmuller, J. *Phys. Rev. B* **1996**, *54*, 11169–11186.
(42) Kresse, G.; Joubert, D. *Phys. Rev. B* **1999**, *59*, 1758–1775.
(43) Perdew, J. P.; Chevary, J. A.; Vosko, S. H.; Jackson, K. A.; Pederson, M. R.; Singh, D. J.; Fiolhais, C. *Phys. Rev. B* **1992**, *46*, 6671–6687.
(44) Monkhorst, H. J.; Pack, J. D. *Phys. Rev. B* **1976**, *13*, 5188–5192.
(45) Henkelman, G.; Jónsson, H. *J. Chem. Phys.* **2000**, *113*, 9978–9985.
(46) Mills, G.; Jónsson, H.; Schenter, G. K. *Surf. Sci.* **1995**, *324*, 305–337.
(47) Henkelman, G.; Uberuaga, B. P.; Jónsson, H. *J. Chem. Phys.* **2000**, *113*, 9901–9904.
(48) Pérez-Cabero, M.; Romeo, E.; Royo, C.; Monzon, A.; Guerrero-Ruiz, A.; Rodríguez-Ramos, I. *J. Catal.* **2004**, *224*, 197–205.
(49) Nagaoka, K.; Jentys, A.; Lercher, J. A. *J. Catal.* **2005**, *229*, 185–196.
(50) Mukainakano, Y.; Li, B. T.; Kado, S.; Miyazawa, T.; Okumura, K.; Miyao, T.; Naito, S.; Kunimori, K.; Tomishige, K. *Appl. Catal., A* **2007**, *318*, 252–264.
(51) Li, D. L.; Shishido, T.; Oumi, Y.; Sano, T.; Takehira, K. *Appl. Catal., A* **2007**, *332*, 98–109.
(52) *Binary Alloy Phase Diagrams*; Massalski, T. B., Okamoto, H., Subramanian, P. R., Kacprzak, L., Eds.; ASM International: Materials Park, OH, 1990; p 2849.
(53) Ruban, A. V.; Skriver, H. L.; Nørskov, J. K. *Phys. Rev. B* **1999**, *59*, 15990–16000.
(54) Christensen, A.; Ruban, A. V.; Stoltze, P.; Jacobsen, K. W.; Skriver, H. L.; Nørskov, J. K.; Besenbacher, F. *Phys. Rev. B* **1997**, *56*, 5822–5834.
(55) Watwe, R. M.; Bengaard, H. S.; Rostrup-Nielsen, J. R.; Dumesic, J. A.; Nørskov, J. K. *J. Catal.* **2000**, *189*, 16–30.
(56) Triantafyllopoulos, N. C.; Neophytides, S. G. *J. Catal.* **2003**, *217*, 324–333.
(57) Abild-Pedersen, F.; Nørskov, J. K.; Rostrup-Nielsen, J. R.; Sehested, J.; Helveg, S. *Phys. Rev. B* **2006**, *73*, 115419–115431.
(58) Albright, L. F.; Marek, J. C. *Ind. Eng. Chem. Res.* **1988**, *27*, 755–759.
(59) Snoeck, J. W.; Froment, G. F.; Fowles, M. *J. Catal.* **1997**, *169*, 250–262.
(60) Snoeck, J. W.; Froment, G. F.; Fowles, M. *J. Catal.* **1997**, *169*, 240–249.
(61) Helveg, S.; López-Cartes, C.; Sehested, J.; Hansen, P. L.; Clausen, B. S.; Rostrup-Nielsen, J. R.; Abild-Pedersen, F.; Nørskov, J. K. *Nature* **2004**, *427*, 426–429.
(62) Klinke, D. J.; Wilke, S.; Broadbelt, L. J. *J. Catal.* **1998**, *178*, 540–554.
(63) Andersson, M. P.; Abild-Pedersen, E.; Remediakis, I. N.; Bligaard, T.; Jones, G.; Engbwk, J.; Lytken, O.; Horch, S.; Nielsen, J. H.; Sehested, J.; Rostrup-Nielsen, J. R.; Nørskov, J. K.; Chorkendorff, I. *J. Catal.* **2008**, *255*, 6–19.
(64) Mavrikakis, M.; Hammer, B.; Nørskov, J. K. *Phys. Rev. Lett.* **1998**, *81*, 2819–2822.
(65) Van Santen, R. A.; Neurock, M. *Russ. J. Phys. Chem. B* **2007**, *1*, 261–291.
(66) Wang, J. H.; Lee, C. S.; Lin, M. C. *J. Phys. Chem. C* **2009**, *113*, 6681–6688.